2008

Recrystallization mechanisms during friction stir welding/processing of aluminum alloys

McNelley, T.R.

Available online at www.sciencedirect.com
ScienceDirect
Scripta Materialia 58 (2008) 349–354
Scripta MATERIALIA
www.elsevier.com/locate/scriptamat

Viewpoint Paper

Recrystallization mechanisms during friction stir welding/processing of aluminum alloys

T.R. McNelley,* S. Swaminathan and J.Q. Su

Department of Mechanical and Astronautical Engineering, Naval Postgraduate School, Monterey, CA 93943-5146, USA

Received 31 July 2007; revised 30 August 2007; accepted 28 September 2007
Available online 26 November 2007

Abstract—Restoration models for hot working of metals and alloys are reviewed in the context of their applicability to friction stir welding (FSW) and friction stir processing (FSP). Two of these models are used to interpret microstructure and microtexture data for two aluminum alloys subjected to FSP. The need for further experiments and model extensions to accommodate the transients and steep gradients in the strain, strain rate and temperature experienced by materials during FSW and FSP are discussed. Published by Elsevier Ltd. on behalf of Acta Materialia Inc.

Keywords: Friction stir welding; Friction stir processing; Dynamic recovery and recrystallization; Particle stimulated nucleation; Microtexture

1. Introduction

The current understanding of restoration (i.e., softening) by recovery and recrystallization during thermomechanical processing of metallic materials has been summarized in several recent monographs and reviews [1–5]. Recent advances in electron microscopy have led to improved understanding of deformation-induced microstructures that develop in pure metals and dilute alloys under nearly uniform, isothermal conditions [6]. For more complex strain paths and alloys, interpretation of microstructures is still largely empirical in nature. Furthermore, under hot working conditions the phenomena involved in restoration are difficult to study and the mechanisms involved are not well understood despite their technological importance.

The recent emphasis on production of ultrafine and nanocrystalline microstructures through severe plastic deformation (SPD) has accentuated the need for models of recrystallization occurring concomitantly with large-strain deformation [7]. However, most of the in-depth studies have involved, again, approximately uniform strains and isothermal conditions during SPD. Friction stir welding (FSW) and friction stir processing (FSP) technologies involve SPD but under conditions that include rapid transients and steep gradients in strain, strain rate and temperature [8,9]. Microstructure transformations and restoration processes in the presence of such transients and gradients have only recently begun to be considered [10–12]. Nevertheless, these processes determine the microstructure and properties of welded or processed materials, and it is imperative to gain better understanding and control of recrystallization in these circumstances.

2. Transients and gradients during FSW/P

The transients and gradients in strain, strain rate and temperature are inherent in the thermomechanical cycles of FSW and FSP. Typically, these processes employ a cylindrical, wear-resistant tool consisting of a smaller-diameter pin that has a concentric larger-diameter shoulder [13]. The tool is rotated as the pin is forced into a location on a surface until the shoulder comes in contact with the material. Heating is due to a combination of friction effects and severe, localized, adiabatic deformation induced in the material by tool rotation. Thus, the heat source is distributed in a volume of deforming material surrounding the pin. This volume of material is usually referred to as the weld nugget in FSW or the stir zone (SZ) in FSP. Once the pin has fully penetrated, the tool may be traversed along abutting edges to accomplish welding of separate work pieces or, conversely, in a pattern on a material surface to accomplish processing. During FSW/P, material flows in a complex pattern around the pin tool from the advancing side

* Corresponding author. E-mail: tmcnelley@nps.edu

1359-6462/$ - see front matter Published by Elsevier Ltd. on behalf of Acta Materialia Inc.
doi:10.1016/j.scriptamat.2007.09.064

(tangential velocity of a point on the tool surface is parallel to the traversing direction) to the retreating side (tangential velocity of a point on the tool surface is antiparallel to the traversing direction). Equilibrium of forces and moments along with the effect of the traversing of the tool dictate that the thermomechanical cycle will also include distinct gradients in the deformation field as well as strain and strain rate transients.

Generally, optical microscopy from transverse sections after FSW/P reveals four distinct regions. First, the weld nugget/SZ comprises the material strongly affected by the tool rotation. Modeling results indicate that the nugget/SZ material has experienced large plastic strains at strain rates in the range 10^1–10^2 s^{-1} [8]. Peak temperatures in this region are thought to be in the range from 0.6 to $0.95T_{Melt}$, depending on the material, tool design and operating conditions, and the upper portions of this region experience heating and deformation effects from the tool shoulder as well as from the tool pin [14–16]. Next is the thermomechanically affected zone (TMAZ), where the material experiences lesser strains and strain rates as well as lower peak temperatures. This region is often characterized by a pattern of grain distortion that suggests shearing and flow of material about the rotating tool. The grain distortion may lead to fragmentation and formation of refined, equiaxed grains near the interface between the TMAZ and the nugget/SZ. Beyond the TMAZ, the heat affected zone (HAZ) experiences only a thermal cycle, and, finally, the base material surrounds the HAZ.

Nugget/SZ microstructures are typically highly refined when compared with the base material. Grains <100 nm in size have been reported in studies of FSP of AA7XXX materials [17] and grain sizes in the range of 1–10 μm have been widely observed in association with FSW/P [15,18]. Combinations of grain size strengthening with strain hardening and other strengthening mechanisms may enable production of fully efficient joints in FSW as well as surface hardening by FSP of materials that are not amenable to conventional heat treatment.

Conventional hot working processes, such as rolling, extrusion and forging, generally involve strain rates in the range 10^0–10^2 s^{-1} at temperatures $\geqslant 0.5T_{Melt}$ but in the absence of the transients and gradients in strain, strain rate and temperature that characterize FSW/P. Nevertheless, models for dynamic restoration during hot working have been employed to interpret microstructures produced by FSW/P techniques [19,20]. Analysis of nugget/SZ and TMAZ microstructures to incorporate such models has led to a variety of interpretations even in otherwise well-studied aluminum alloys. Different models and their applicability to FSW/P are reviewed in the following paragraphs. An example is also provided of recent microstructure and microtexture analysis for two aluminum alloys displaying two distinct classes of behavior, and their interpretation based on conventional models.

3. Dynamic restoration during hot working

Restoration processes that take place concurrently with deformation are classified as dynamic in order to distinguish them from processes that take place during static annealing [3]. The latter may occur during cooling after completion of deformation or between successive stages of deformation during FSW/P.

Dynamic recovery (DRV) occurs readily during hot working of metals of high stacking fault energy such as aluminum [3,5,21]. The flow stress rises during the initial stage of deformation as dislocations multiply and interact. However, the rate of recovery also increases as the dislocation density increases and dislocations begin to rearrange and form low-angle boundaries as subgrains develop. Eventually, the flow stress saturates as hardening due to dislocation multiplication and recovery due to dislocation rearrangement reach a dynamic equilibrium. This leads to deformation at a steady state wherein the flow stress remains constant with strain. The steady state is reflected in equiaxed subgrains with nearly dislocation-free interiors, constant subgrain size and subgrain boundary misorientation. The steady state appears to reflect continual processes of subgrain boundary formation, rearrangement and dissolution during deformation. During DRV, the flow stress, dislocation structure and texture evolution depend on the Zener–Hollomon parameter, $Z = \dot{\varepsilon}\exp(Q/RT)$, where $\dot{\varepsilon}$ is the strain rate, Q is an activation energy and R and T have their usual meaning. Thus, the flow stress and dislocation density increase while the subgrain size decreases when Z increases. Deformation textures form and persist throughout straining, although the relative strengths of various deformation texture components depend on alloy composition and Z. At moderate strains in the steady state the prior grains retain their identity and change shape while dislocation and subgrain structures remain approximately constant. At very large strains the separation of the prior boundaries may be reduced to the subgrain size; this circumstance will be considered separately. DRV reflects the ease of climb and cross-slip in materials of high stacking fault energy; corresponding deformation microstructures tend to be homogeneous, and the absence of local strain concentrations apparently precludes alternative restoration mechanisms. Alloying additions to aluminum do not have an appreciable effect on the stacking fault energy and so DRV is expected to predominate in aluminum materials under hot working conditions.

Discontinuous dynamic recrystallization (DDRX) occurs in metals of moderate to low stacking fault energy during hot deformation [3]. In DDRX, new, dislocation-free grains form at sites such as prior grain boundaries, deformation band interfaces or boundaries of newly recrystallized grains. In DDRX, the driving force for initiation of recrystallization is the strain-induced build up of stored strain energy in the form of fine cells and a high free dislocation density. During deformation, a low stacking fault energy retards the climb and cross-slip processes of DRV, thereby enabling the formation of stable grain nuclei at various sites in the deformation microstructure. The newly formed grains deform as they grow, and the build up of stored strain energy in the new grains may reduce the driving force for their continued growth but increase the frequency of initiation of new grains. A ''necklace'' structure of newly formed grains may result when prior grain boundaries

are the initiation sites for DDRX. Beyond a critical strain for initiation, DDRX may lead to cyclic softening and hardening in the stress–strain curve. This mechanism is usually observed when deformation temperatures are greater than $0.3T_{\mathrm{Melt}}$ and is accompanied by the replacement of deformation textures with characteristic recrystallization textures. A condition for initiation of DDRX may be given by

$$\frac{\rho_{\mathrm{m}}^3}{\dot{\varepsilon}} > \frac{2\gamma_{\mathrm{b}}}{KLMGb^5} \tag{1}$$

where ρ_{m} is the mobile dislocation density, $\dot{\varepsilon}$ is the strain rate, γ_{b} is the grain boundary energy, K is a constant fraction of the dislocation line energy that is stored in the newly formed grains, L is mean slip distance of dislocations in these grains, M is the boundary mobility, G is the shear modulus and b is the Burger's vector. This inequality suggests a strong dependence of the conditions for DDRX on the mobile dislocation density: a low stacking fault energy tends to suppress recovery, leading to high values of ρ_{m}. In contrast, for materials of high stacking fault energy, recovery reduces ρ_{m}, thereby precluding DDRX, especially at high strain rates. When slip contributions to straining are inhibited by restricted numbers of slip systems or by solute drag effects, and boundary migration is likewise retarded by solute, lattice rotation may develop progressively at grain boundaries as dislocations accumulate during straining. This may lead to dynamic recrystallization by lattice rotation as new grains form at prior boundaries, and a necklace structure similar to that often observed in DDRX.

The onset of geometric dynamic recrystallization (GDRX) may be observed as the strain increases during DRV when the separation of prior boundaries approaches the subgrain size [3,5,22]. The boundary separation in the normal direction, d_{N}, during hot or warm rolling may be taken as $d_{\mathrm{N}} \cong d_0\exp(-\varepsilon)$, where d_0 is the initial grain size and ε is the strain. Prior boundaries become serrated as they respond locally to the interface tensions of subgrain boundaries and develop waviness over distances on the order of the subgrain size. Then, GDRX may occur when the prior boundary separation becomes equal to the subgrain size, which, in turn, is related to Z^{-1}. Thus, at low strain rates and stresses, the small values of Z will lead to the onset of GDRX at small strains, while at high strain rates and stresses the DRV stage of deformation will be more prolonged prior to the onset of GDRX. However, the recrystallized grain size will be finer when deformation takes place at higher values of Z. During rolling deformation the transformation of elongated, lamellar grains that contain subgrains into a recrystallized grain structure by GDRX apparently involves rearrangement of boundary nodes under the influence of interface tensions, and the resulting grains are surrounded by a mixture of prior boundary segments and subgrain boundaries. Because GDRX does not involve long-range migration of high-angle boundaries, the prior deformation texture is retained during the transformation to a grain structure.

Recrystallization via particle stimulated nucleation (PSN) involves the formation and growth of new grains from fine cells or subgrains in the deformation zones developed around dispersed particles during prior straining [23]. Non-deforming particles must be accommodated during plastic flow by the generation of geometrically necessary dislocations. When particles exceed a size of about 0.1 μm, highly misoriented cells or subgrains form in zones surrounding the particles. For a particle, the size of the deformation zone scales with the particle size and also grows larger as strain increases, and a particle may serve as a nucleation site when a stable nucleus can form within the surrounding deformation zone. With sufficient stored strain energy in the matrix the critical particle diameter for nucleation decreases as the strain increases. Typically, particles must exceed a size of about 0.5 μm for PSN. During hot working, recovery will reduce the dislocation density in deformation zones and the surrounding matrix; nevertheless, deformation zones may still form around particles of size exceeding a value, d_{f}, that may be estimated from the relationship

$$d_{\mathrm{f}} \geqslant \left(\frac{K_1}{TZ}\right)^{1/2} \tag{2}$$

where K_1 is a material constant ($\sim$1712 $\mathrm{m^2\ K\ s^{-1}}$ for aluminum alloys [3]). The new grain must also be able to grow; the particle size that must be exceeded in order for growth to occur has been estimated as

$$d_{\mathrm{g}} \geqslant \frac{4\gamma_{\mathrm{b}}K'Gb}{3\gamma_{\mathrm{s}}Z^{1/m}} \tag{3}$$

where γ_{b} and γ_{s} are the grain boundary and subgrain boundary interfacial energies, respectively, K' is a material constant and m is the stress exponent for elevated temperature deformation (typically, $0.1 \leqslant m \leqslant 0.5$). Both conditions must be satisfied for PSN during or immediately after hot working, and so the formation condition predominates at lower Z while the growth condition predominates at higher Z. Grain growth may also occur if time-at-temperature is sufficient. A distinguishing characteristic of PSN is that recrystallization textures tend to be random, or have very weak deformation components [10].

4. Recrystallization mechanisms in FSW/P

The foregoing models were developed from experiments involving conditions of approximately uniform straining and isothermal deformation conditions. Studies of hot working have often employed hot compression or hot torsion testing methods that may enable investigation of strain and strain rate regimes overlapping those of FSW/P. Results of hot torsion simulations of FSW of AA7010 have been interpreted in terms of nugget grain refinement by GDRX [24]. Nevertheless, the ultrafine grain size observed in the FSW nugget could only be explained by invoking heterogeneous flow in the nugget in order to achieve local strains and strain rates sufficient to account for the observed grain sizes, and simulation of such heterogeneous flow is not feasible. Furthermore, the potential contributions of the steep gradients in strain, strain rate and temperature

that are characteristic of FSW/P could not be replicated by hot torsion methods.

Numerous investigations of FSW-induced microstructures in aluminum alloys have been conducted in the last decade. Microscopy techniques have included microtexture and orientation imaging microscopy (OIM) methods, as well as optical and transmission electron microscopy (TEM) techniques. For example, a study designed to examine microstructures at locations surrounding the FSW tool has shown that subgrains form ahead of the tool and develop greater misorientations at locations nearer the tool [25]. However, regions in the nugget that were adjacent to the pin tool were difficult to characterize because electron backscatter diffraction pattern quality becomes severely degraded due to residual strain. This is, again, a reflection of the steep strain and strain rate gradients in such locations, and the material that has undergone the most severe deformation likely has the greatest effect on the final nugget microstructure. Tool plunge and extract experiments followed by static annealing have sought to replicate the thermomechanical cycles of FSW/P. In AA7050 grains 25–100 nm in size were observed after tool extraction and subsequent static annealing resulted in grains 2–5 μm in size [26]. These measurements were made on samples obtained at the bottom of the extraction site and were unaffected by tool translation. Conditions during a plunge and extract experiment followed by static annealing will not fully replicate microstructure evolution during FSW/P.

Altogether, DRV, GDRX and DDRX have been cited as the mechanisms that can account for grain refinement in FSW/P in aluminum and various aluminum alloys [11,12,20,24,25]. The two former mechanisms are consistent with the current understanding of recrystallization in aluminum in light of its high stacking fault energy. However, DDRX, which has been cited in studies of FSP of AA7075, is inconsistent with the high stacking fault energy of aluminum [12]. Nevertheless, ultrafine grains (<100 nm in size) have been observed in TEM investigations of this alloy for selected processing conditions.

Microtexture results have been reported along with microstructures produced by FSW/P in several studies, but systematic examinations of texture evolution, restoration mechanisms and processing conditions remain to be carried out for aluminum materials. A schematic of multi-pass FSP is shown in Figure 1, wherein the tool traverses in the *X*-direction. Two results from separate investigations in this laboratory of FSP applications in aluminum alloys are summarized in Figures 2 and 3, and illustrate two broad categories of behavior. In both cases, the data were acquired on transverse planes (i.e., the *Y*–*Z* plane in Fig. 1) after completion of processing, and so they represent the overall effect of the FSP thermomechanical cycle and do not provide details of microtexture and microstructure evolution during the course of processing. Figure 2a shows an inverse pole figure (IPF) map, image quality (IQ) map and complete 0 0 1, 0 1 1 and 1 1 1 pole figures from a location at the mid-depth of the SZ for multi-pass FSP (at 400 rpm/5 ipm, with successive passes separated by 5 mm) using a 12 mm step-spiral MP159 steel tool on a rolled AA2099-T8 plate 12.7 mm in thickness. The nominal alloy composition is Al–2.3Cu–1.66 Li (in wt.%). The IPF and IQ maps show grains having a mean linear intercept (MLI) size of ~5 μm and containing few discernible second-phase particles. The dark lines in these maps represent high-angle boundaries (>15° misorientation). The pole figure data may be interpreted in terms of a shear texture involving a distinct B-fiber component if it is assumed that the transverse plane (i.e., the *Y*–*Z* plane) is the shear plane and that the shearing direction is nearly aligned with the *Y*-direction. This implies that the location in Figure 2 was near the center of a pass. Despite the small number of grains apparent in Figure 2, the

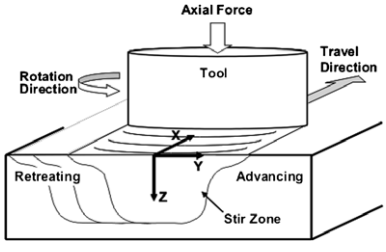

Figure 1. A schematic representation of multi-pass FSP, including the axes for description of microstructure and texture. The *Y*–*Z* plane is transverse to the direction of tool advance.

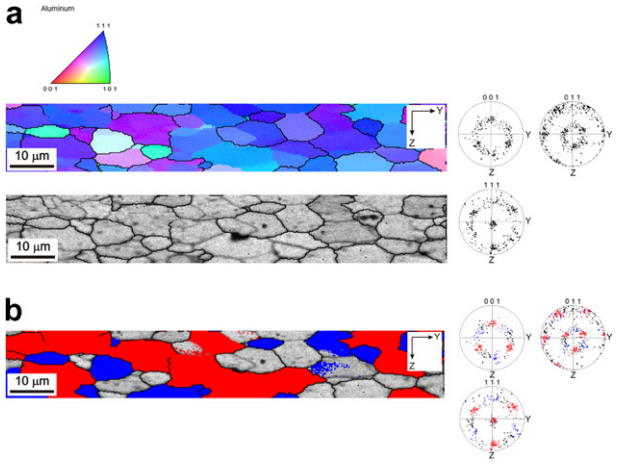

Figure 2. (a) IPF and IQ maps of a region on the transverse plane in the SZ for multi-pass FSP of AA2099 material showing refined grains about 5 μm in size; the discrete pole figures show a distinct shear texture in the location of these maps. (b) The two variants of a B-type shear texture component highlighted in the IQ map and pole figures. High-angle boundaries separate these variants.

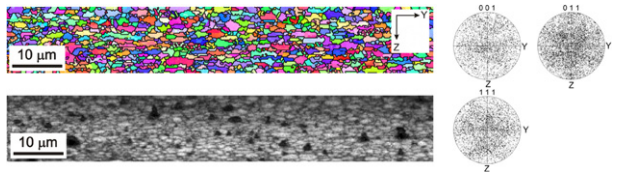

Figure 3. IPF and IQ maps of a region on the transverse plane in the SZ for multi-pass FSP of as-cast, continuously cast AA5083 material showing refined grains ~1 μm in size. The discrete pole figures show that the texture is nearly random at this location.

texture is quite distinct at this location. Furthermore, it is possible to discern the two variants of this shear texture component, as demonstrated by use of different colors to highlight each variant in Figure 2b. Corresponding highlighting of the IQ map is also shown in Figure 2b, wherein high-angle interfaces are observed to separate the texture variants.

Figure 3 shows data for multi-pass FSP of an as-cast, continuously cast AA5083 plate 15 mm in thickness. The nominal alloy composition is Al–4.7Mg–0.7Mn. In this example, the FSP was conducted at 350 rpm/4 ipm, with a separation between successive passes of 2 mm and using a step-spiral H13 steel tool having a pin length of 5.2 mm. It is noteworthy that the grain size achieved in this case is ~1 μm. This is apparent in both the IPF and IQ maps, and dark lines again delineate the high-angle boundaries. The dark areas in the IQ map suggest the presence of dispersed particles in an apparent volume fraction greater than in the AA2099 material. The nearly uniform distribution of orientations in the pole figures for this region indicate the presence of a nearly random texture, in contrast to the strong shear texture seen for the AA2099 material in an identical scan area. Thus, the data of Figures 2 and 3 suggest two distinctly different mechanisms of microstructure and texture evolution in these examples.

The retention of a shear-type deformation texture within the SZ of the AA2099 material after multi-pass FSP suggests that the DRV and GDRX mechanisms dominate processes of microstructure refinement. While these mechanisms may account for grains 5 μm in size, it is difficult to understand the formation of 100 nm grains [17] by these mechanisms at the nugget/SZ temperatures anticipated. In contrast, the presence of a random texture in the SZ after multi-pass FSP of as-cast, continuously cast AA5083 indicates that PSN during or immediately after passage of the tool is a plausible mechanism for grain refinement in this case. This may be shown by plotting the particle size, d_f, for formation of deformation zones around particles as a function of SZ temperature in the interval of $0.7–0.9T_{Melt}$ (400–550 °C) according to Eq. (2). This is shown in Figure 4. Two different strain rates, 10^1 and 10^2 s^{-1}, were used in this calculation; the formation criterion dominates for most of the range represented by these rates and temperatures. For a strain rate of 10^2 s^{-1}, the particle size, d_f, for zone formation increases from about 0.5 μm at 400 °C to 4.5 μm at 550 °C. Coarser particle sizes for zone formation are obtained at lower strain rates. While the PSN model can account for the texture, it is difficult to account for the highly refined grain size observed here unless particles are more efficient nucleation sites than normally expected [3].

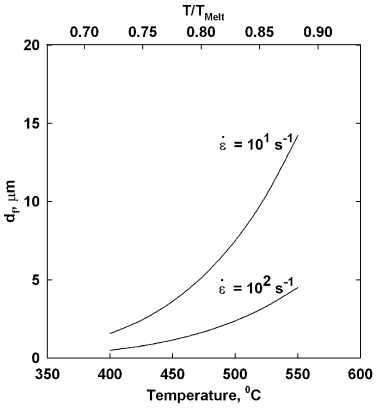

Figure 4. Plots of the critical particle size for deformation zone formation, d_f, as a function of nugget/SZ temperature for two strain rates according to Eq. (2) [3].

5. Summary

Though two different plausible mechanisms have been identified in determining the SZ microstructures of AA2099 and AA5083 after FSP, it has to be recognized that these results were obtained on the materials that had different initial conditions and were subjected to different processing as well as tool parameters. Further, the observations were made on the transverse plane after the tool had passed, a plane of observation employed in a majority of studies. Only a few studies have been performed using "quick-stop" and tool extraction techniques, wherein the tool is withdrawn and the material rapidly quenched prior to examination throughout the nugget/SZ [11,12,25,26]. Such studies have highlighted the possibility that a combination of models is necessary to describe the different microstructures observed. Future efforts should employ such techniques on a variety of alloys to examine both process and alloy constitution effects on the operative mechanism(s). Also, the conventional models of restoration need to incorporate the transients and steep gradients associated with FSW/P.

Acknowledgements

The authors acknowledge partial support for this work under funding document N0001407WR20053 from the Office of Naval Research (ONR), with Dr. Julie Christodoulou as program monitor. S.S. and J.Q.S. also acknowledge the support of the US National Research Council (NRC) Research Associateship program.

References

[1] P. Cotterill, P.R. Mould, Recrystallization and Grain Growth in Metals, Surrey University Press, London, 1976.
[2] J.G. Byrne, Recovery, Recrystallization and Grain Growth, McMillan, New York, 1965.
[3] F.J. Humphreys, M. Hatherly, Recrystallization and Related Annealing Phenomena, Elsevier, Oxford, 2004.
[4] J.J. Jonas, C.M. Sellars, W.J. McG. Tegart, Met. Revs. 130 (1969) 1.
[5] R.D. Doherty, D.A. Hughes, F.J. Humphreys, J.J. Jonas, D. Juul Jensen, M.E. Kassner, W.E. King, T.R. McNelley, H.J. McQueen, A.D. Rollett, Mater. Sci. Eng. A 238 (1997) 219.
[6] G.I. Rosen, D. Juul Jensen, D.A. Hughes, N. Hansen, Acta Metall. Mater. 43 (1995) 2563.
[7] F.J. Humphreys, P.B. Prangnell, J.R. Bowen, A. Gholinia, C. Harris, B. Hutchinson, L.M. Brown, M.J. Stowell, J. Gil Sevillano, P.J. Withers, Philos. Trans. Roy. Soc. Lond. A 357 (1999) 1663.

[8] A. Askari, S. Silling, B. London, M. Mahoney, in: K.V. Jata, M.W. Mahoney, R.S. Mishra, S.L. Semiatin, D.P. Field (Eds.), Friction Stir Welding and Processing, TMS, Warrendale, PA, 2001, pp. 43–50.
[9] D.P. Field, T.W. Nelson, Y. Hovanski, K.V. Jata, Metall. Mater. Trans. A 32 (2001) 2869.
[10] K. Oh-Ishi, A.P. Zhilyaev, T.R. McNelley, Metall. Mater. Trans. A 37 (2006) 2239.
[11] P.B. Prangnell, C.P. Heason, Acta Mater. 53 (2005) 3179.
[12] J.Q. Su, T.W. Nelson, C.J. Sterling, Mater. Sci. Eng. A 405 (2005) 277.
[13] W.M. Thomas, E.D. Nicholas, J.C. Needham, M.G. Murch, P. Templesmith, C.J. Daws, G.B. Patent Application No. 9125978.8, December 1991, US Patent No. 5460317, October 1995
[14] K. Oh-Ishi, T.R. McNelley, Metall. Mater. Trans. A 35 (2004) 2951.
[15] Y.S. Sato, M. Urata, H. Kokawa, Metall. Mater. Trans. A 33 (2002) 625.
[16] C.G. Rhodes, M.W. Mahoney, W.H. Bingel, R.A. Spurling, C.C. Bampton, Scripta Mater. 36 (1997) 69.
[17] J.Q. Su, T.W. Nelson, C.J. Sterling, J. Mater. Res. 18 (2003) 1757.
[18] Z.Y. Ma, S.R. Sharma, R.S. Mishra, Mater. Sci. Eng. A 433 (2006) 269.
[19] K.V. Jata, S.L. Semiatin, Scripta Mater. 43 (2000) 743.
[20] J.Q. Su, T.W. Nelson, R. Mishra, M. Mahoney, Acta Mater. 51 (2003) 713.
[21] H.J. McQueen, W. Blum, Mater. Sci. Eng. A 290 (2000) 95.
[22] H.J. McQueen, O. Knustad, N. Ryum, J.K. Solberg, Scripta Metall. 19 (1985) 73.
[23] F.J. Humphreys, P.N. Kalu, Acta Metall. Mater. 35 (1987) 2815.
[24] K.A.A. Hassan, B.P. Wynne, P.B. Prangnell, In: Fourth International Symposium on FSW, Park City, UT. TWI, 2003 (cd rom).
[25] R.W. Fonda, J.F. Bingert, K.J. Colligan, Scripta Mater. 51 (2004) 243.
[26] C.G. Rhodes, M.W. Mahoney, W.H. Bingel, M. Calabrese, Scripta Mater. 48 (2003) 1451.